

HIGH EFFICIENCY LASER-ASSISTED H⁻ BEAM CONVERSION TO PROTONS

written by

David Lewis Brown

Submitted to the faculty of the University Graduate School

in partial fulfillment of the requirements

for the degree of

Master of Science

in the Department of Physics,

Indiana University

2008

Accepted by the Graduate Faculty, Indiana University in partial fulfillment of the requirements for the degree of Master of Science.

SY Lee, Ph.D., committee chair

Stuart Henderson, Ph.D., student advisor

Masters
Committee

W. Michael Snow, Ph.D.

Rex Tayloe, Ph.D.

2008

Copyright © 2008
David L. Brown
ALL RIGHTS RESERVED

Acknowledgements

The Laser-Stripping project has been a central focus in my career for two years, and there are many people to thank, many of whom were necessary for this work to be possible. I would like to thank my wife, Sharon, and my daughter, Amelia, for their endless patience with me while I spent the necessary time in school for two weeks at a time, and extra work hours put in for the project at work. Thank you to Stuart Henderson and Saeed Assadi for allowing me to work on the Laser project at the Spallation Neutron Source at the Oak Ridge National Laboratory. For their encouragement and guidance as I struggled to maintain focus while juggling a busy work schedule, I will forever be indebted. In addition, I would like to thank Viatcheslav Danilov, Warren Grice, and Yun Liu for their contributions to the project in general and their contributions to my informal education in the Accelerator Physics and the Laser Physics aspects of the project. I would be remiss if I failed to mention William Barletta, Helmut Wiedemann, and S.Y. Lee, past and present directors of the USPAS, Susan Winchester, and Marilyn Paul, staff of the USPAS office, and all of the USPAS instructors for offering the opportunity for such an endeavor and the unrelenting desire to see students of the USPAS succeed. Last, but certainly not least, a special thanks goes out to my immediate supervisors and coworkers who have worked diligently to ensure my attendance at the USPAS courses was not impeded, and that I had sufficient time to donate to special projects like the Laser-Stripping experiment.

Abstract

David L. Brown

High-Efficiency Laser Assisted H^- Beam Conversion to Protons

A proof-of-principle experiment to prove the viability of converting H^- to H^+ through a 3-step, laser assisted, high-efficiency stripping method has been performed with exceptional results. This new stripping method has the potential to allow further increases in beam power to be obtained at high-intensity proton facilities by eliminating limitations associated with carbon foils. In addition, the laser technology used is robust and reliable.

Contents

1. Introduction/ Motivation of the Experiment.....	1
2. Multi-turn Charge Exchange Injection.....	4
2.1. Foil Limitations.....	5
2.2. Laser Stripping Prospects.....	9
3. Laser Assisted Stripping with a Nanosecond Laser.....	11
3.1. Atomic Physics of a Hydrogen Atom.....	11
3.2. Photo-Excitation.....	15
3.3. Doppler Shift and Doppler Broadening.....	20
3.4. Experimental Theory.....	21
3.5. Charged Particle Response to Magnetic Stimuli.....	23
4. Experimental Setup.....	27
4.1. Facilities.....	27
4.2. Front End and Linac.....	28
4.3. Experimental Layout.....	30
4.4. Ion Beam Optics, Laser Beam Layout, and Optics of Laser.....	32
5. Results of the Experiment.....	38
6. Conclusions & Future of the Project at the SNS.....	45
7. References.....	47

Chapter 1

Introduction/Motivation of the Experiment

In many proton accelerators, an accumulation ring is used for the purpose of increasing the current per pulse delivered to the end user. This is especially true in the field of Neutron Sciences where there is a fervent desire to increase the current, beam power, and the brightness of the neutron beam which yields higher resolution neutron scans.

A common method of stacking the proton beam in the accumulation ring is to utilize the charge exchange between an H^- beam and H^+ beam to meld the two beams. Thin carbon or diamond foils are, then, used to strip the electrons, converting all beams into a proton beam. With the increasing prevalence of high-intensity proton beams, as in the Spallation Neutron Source, the carbon foil method becomes inadequate due to the increased radioactivity, the chance of foil failure ever increasing, inefficiency of the foils, and uncontrollable beam loss produced, which is one of the primary beam power limitations in high-intensity proton rings.

Radioactivity, in general, is a common concern for particle accelerators, so much so that policies and practices are developed to reduce the amount of radiation produced from the machine. A major area of focus to reduce this potentially dangerous energy is machine design, specifically to reduce loss. It should be obvious that any intercepting device that blocks beam transport, partially or completely, contributes in large part to the radioactivity of the

machine in that area. As higher energy and more intense beam is being sought in High Energy Physics, minimizing intercepting devices in the design is desirable. The carbon foil method utilizes a thin insertable foil that strips the beam as the foil is encountered, and it stands to reason that the more particles that pass through the foil, the more radiation is produced from that intercepting device.

In addition to radioactive concerns, the foil itself is a liability as it has a lifetime limitation which is determined by the heat generated by the beam as it passes through the foil. Continuous heating and cooling of the foil leads to embrittlement and eventual deterioration of the material (i.e. foil failure) [1, 2].

Foil efficiency, which can range from 90-98%, is restricted in that it is nearly impossible to strip the entire beam with the foil because of physical limitations. In order to strip a particle beam of its existing electrons with the foil, one must ensure that the location of the particle beam on the foil is accurate enough so as to maximize the stripping effect. Additionally, one must make sure that the beam size at the foil is sufficiently large to distribute the inherent heat load deposited by the beam across the foil.

Uncontrollable losses contribute significantly, as well, to the concern of using carbon foils in future machines through nuclear scattering, energy straggling, and multiple scattering. Nuclear interactions would naturally affect the trajectory of the particles being stripped, but the less obvious byproducts of the stripping foil is a decrease in energy caused by the interaction with the foil which, in turn, causes circulating beam to be lost as the energy differs from the ideal energy for the accumulation ring. In addition, there is an increase in

transverse emittance caused by the foil interaction which, again, causes losses as the beam size and shape, not to mention the halo, increase to the point where the admittance is too small to contain the beam.

The foils used also have a 2 MW power limit beyond which the foil begins to ablate or deform until the foils cease being useful [3]. All of these issues limit the usefulness of the stripping foil method against the backdrop of ever higher powers being sought at such projects as the European Spallation Neutron Source.

An alternate, more efficient method of stripping is the 3-step, laser assisted, high-efficiency conversion from H^- to protons, which has been recently shown to be ~98% efficient [4]. H^- ion laser stripping was initially proposed by Zelensky, *et al*, in a paper [5] describing a 3-step stripping method: H^- atoms are converted to H^0 , causing the remaining electron's excitation from ground to upper state through energy introduction, and H^0 conversion to H^+ through the photo-ionization process. Our experiment modified the first and third steps of this process by employing a strong magnetic field to utilize Lorentz Stripping instead of the photo-ionization process, and modified the second step to more effectively populate the excited state. It is the hope of the project that the laser stripping technique will replace the more common carbon foil method.

Chapter 2

Multi-turn Charge Exchange Injection

Accelerator physicists aspire to achieve higher power particle beams, be it proton, electron, or heavy ion beam, for various reasons. Motivations range from increasing collision energy to search for theoretical particles to generating higher power ultra-violet laser beams to producing higher power and higher flux neutron beams for the purpose of probing material characteristics. One common method to deliver higher power protons to the target is increasing the current, and can be achieved in two common ways; increasing the source current or combining several beam pulses into a larger beam pulse.

Obviously, an increase in the current emanating from the source will increase the particle throughput, but this scheme is limited and difficult as increasing current from a source introduces power issues, cooling issues, and longevity. A more common and easier way of increasing the current is using an accumulator ring which uses a multi-turn charge exchange method to take beam from an injector and unite incoming beam with the circulating beam. In order to achieve this combination, a carbon foil is routinely utilized to strip electrons from H^- particles and send the resultant H^+ particles around the ring to interact with the incoming beam before the carbon foil (Fig. 2-1).

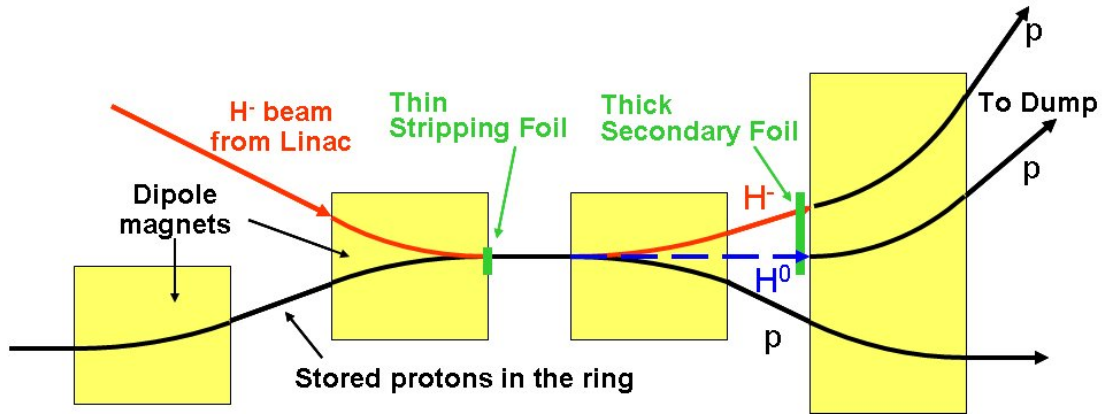


Figure 2-1 - Injection region layout as designed for the Spallation Neutron Source

These beams then pass through the stripping device again to strip the electrons off the H⁻ yielding a completely H⁺ beam. This process, known as stacking, is performed over many Ring turns, until the current desired is achieved.

2.1. Foil Limitations

Limitations of stripping foils are spelled out briefly in the introduction, but I will lay out a more in depth explanation, here. Beam loss and heating are the foremost issues with carbon foils. If we assume the parameters from Table 2-1 and assume $300 \mu\text{g}/\text{cm}^2$, we can take some results from J. Beebe-Wang, et al [3].

Beam Kinetic Energy	1 GeV
Protons per Pulse	2.08×10^{14}
Stripping Foil Size	$6\sigma_{inj}$
Horizontal tune ν_x / Vertical tune ν_y	6.3 / 5.8
Injected beam Emittance	$0.5 \pi\text{mm-mr}$
Un-norm. Painted beam Emittance	$120 \pi\text{mm-mr}$

Table 2-1 – Reproduced from [3] for the purpose of defining the parameters for the model

The two types of beam loss in the injection region (controlled and un-controlled) are defined by the following:

Controlled Beam Loss – Beam particles which miss the foil or are not fully stripped but can be directed to the Injection Dump

Uncontrolled Beam Loss – Beam particles which scatter in the foil and are not captured resulting in a source of radiation in the injection region.

Uncontrolled beam loss will not be discussed at length here as this is not a major factor in the lifetime of the foil, but is rather a phenomenon which is a product of the foil intersecting the beam. In that regard, uncontrolled beam loss is useful in demonstrating one aspect of carbon foils which is undesirable as it increases the localized radioactivity of the injection region.

Contributing factors to controlled beam loss are tuning errors which missteer the center of the beam and non-ideal emittance, or distribution, of the beam on the foil. Naturally, emittance of the beam at the foil correlates to loss (Fig. 2-2) as the larger the emittance of the beam the more beam misses the foil. However, emittance is also proportional to the heat load on the foil (Fig 2-3) as a direct result of the density of the beam deposited in localized regions on the foil.

Fig. 2-4 depicts the two basic painting schemes, or ways to join incoming beam with a core of circulating beam, considered when the calculation of the maximum heat capacity of the foil is done; the schemes are a) anti-correlated and b) correlated. Painting schemes are important to characterize as this determines the number of times the circulating beam interacts with the foil. According to J. Beebe-Wang, et al [3], the maximum foil temperature for the anti-correlated

painting scheme is 2378K in the model in [3] and is higher than the maximum foil temperature for the correlated painting scheme which is 2243K. The lifetime of the foil has been demonstrated at Brookhaven National Laboratory to be around 78 hours at these temperatures but falls off sharply as the temperature increases beyond 2500 K [3]. The most likely foil failure that the SNS injection region has seen is curling of the foil as the structural integrity of the material erodes over time due to heat stress. Another very common foil failure seen at other facilities is ablation which is caused by acute heat deposits which cause a localized heating of the foil and structural breakdown manifests in foil particles sputtering from the surface resulting in a perforation of the material.

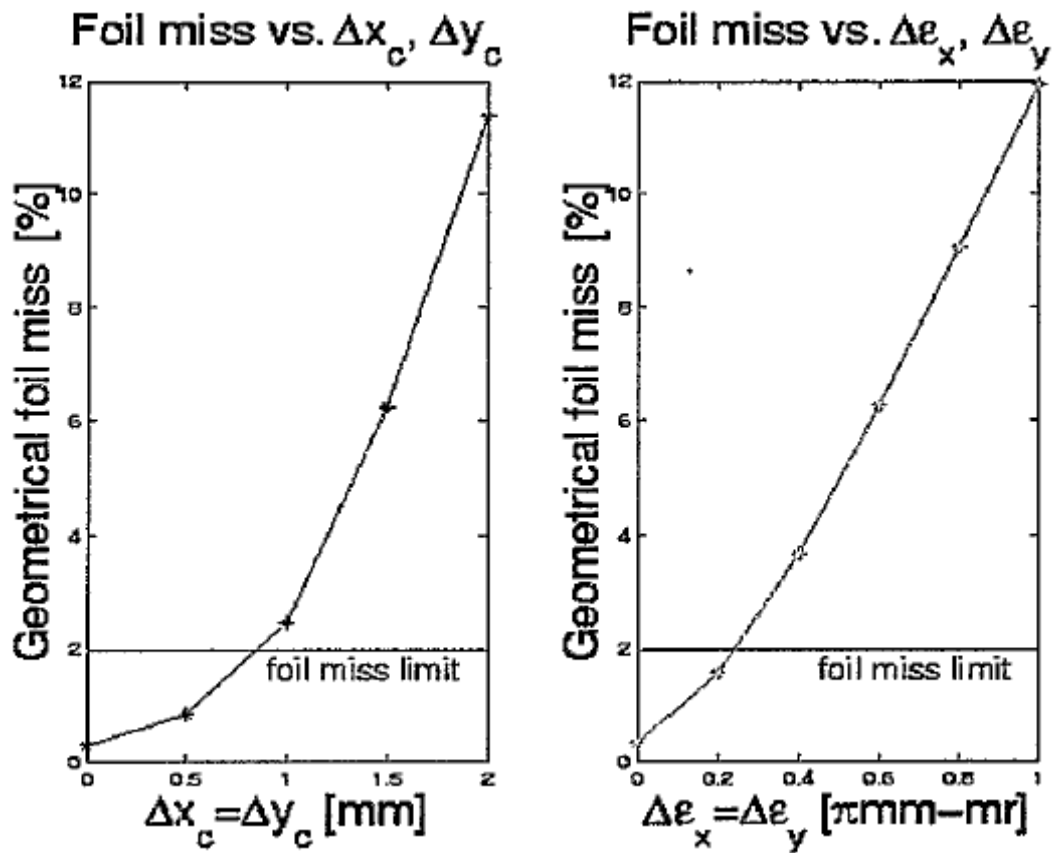


Figure 2-2 – relationship of emittance to % beam missing foil (reproduced from [3])

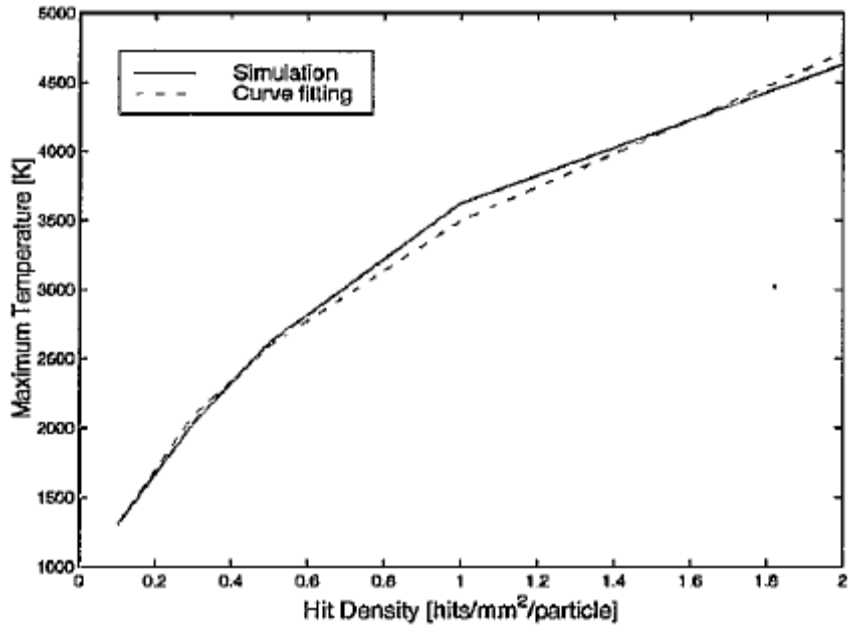


Figure 2-3 – Foil temperature vs. beam current density deduced from the model spelled out in and the curve fit used in foil temperature distribution studies (reproduced from [3]).

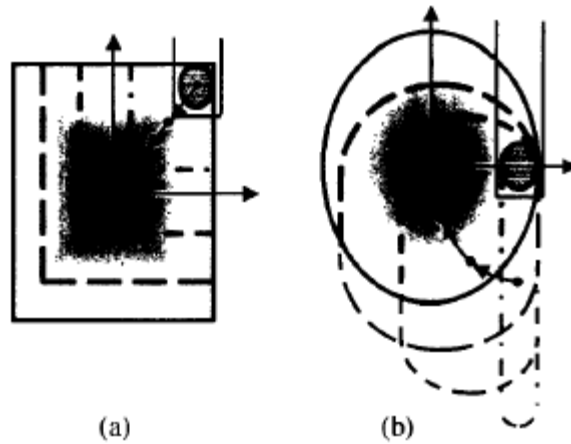


Figure 2-4 – a) anti-correlated painting and b) correlated painting schema (reproduced from [5])

Additional to the lifetime problems resulting from emittance deviation is the foil efficiency which is characteristic of the stripping material. During injection, a fraction, sometimes small and sometimes not so small, of the H^- beam hitting the foil does not get stripped and does not get deflected, but joins the H^- beam which misses the foil and is directed to the Injection Dump. In addition, some of the beam which strikes the foil gets single stripped to H^0 which gets

direction to the Injection Dump, as well, but on a different trajectory. The efficiency of a foil is directly proportional to the thickness of the foil. For a foil with thickness of 200-400 $\mu\text{g}/\text{cm}^2$, the efficiency is about 90-98 %, which cannot be easily overcome. Fig. 2-5 shows the style of the diamond foil at the SNS.

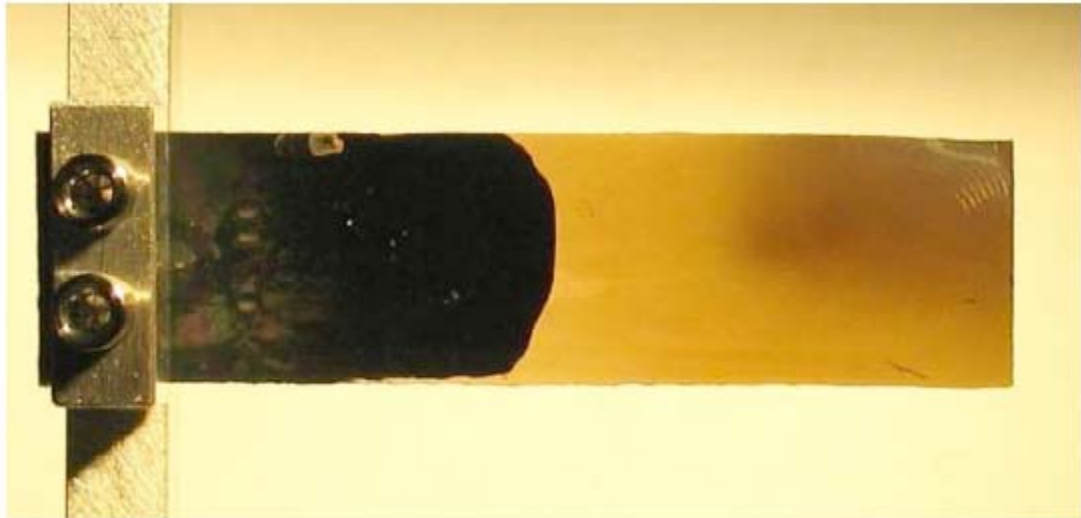


Figure 2-5 – A mixed slurry of diamond particulates in an ultrasonic bath was used for the pre-growth substrate roughening to create diamond nucleation sites. The 12x20 mm² foil depicted above shows damage on the darkened, upper right hand corner of the foil after a three month run period of about 60 kW beam (the SNS has achieved 500 kW + beam as of this writing) (recreated from [2]).

Efficiencies and lifetime issues combined with the radiation generated in that region create the urgency to develop a new way of stripping that addresses all of these issues as the neutron science community pushes to exceed the limitations of these devices.

2.2. Laser Stripping Prospects

Optical stripping schemes are promising to replace the carbon foil stripping method as the dominant way to strip electrons in future particle accelerators. In the course of developing a feasible design for laser-based

stripping, there have been a few iterations which lead to the recent developments which are the basis of this paper: The Zelensky method and the Yamane Method.

Zelensky Method - A “foil-less” charge exchange injection method was proposed by Zelensky, et al [6] which employed a photo detachment or field dissociation process to free the first electron. Next a laser was used to excite the hydrogen atom and to ionize the beam through photo-ionization. The laser power needed to fulfill the requirements for this scheme far exceeds practicality, as the technology to commercially build a laser which supplies sufficient power at the desired beam size for complete photo detachment does not exist, at the time of this writing. In addition, a laser which could produce such powers would have to be specially made and cost much more than commercially available lasers.

Yamane Method - Another, more practical alternative was proposed by Yamane [7] which stripped the H^+ ion of the first electron in a strong dipole field through Lorentz Stripping, using the laser to excite the atom to the $n=3$ state from $n=1$, and then using a second, and final strong dipole field to finish the stripping process. The Doppler shift seen by the H^0 beam, however, would increase the hydrogen absorption linewidth of the beam to a level which is well beyond that which lasers of the day can compensate. Another difficulty presented, as well, is that the momentum spread of the H^+ beam is finite and not stripped efficiently by a monochromatic laser beam. This means only a small fraction of the beam would be excited to the $n=3$ state.

Chapter 3

Laser-Assisted Stripping with a Nanosecond Laser

The proposal of Danilov, et al, [4] includes all of the design features of the Yamane model with an additional design enhancement to address the issues of inefficiently stripping polychromatic particle beam with monochromatic lasers. The improvement requires the laser to diverge as it approaches the beam and the small incidence angle changes would correspond to a small momentum deviation from the idealized momentum. This small correction, as we will see in the subsequent sections of this paper allows the calculated efficiency of the system to increase from a very small percentage to ~98% [4].

3.1. Atomic Physics of the Hydrogen Atom

In order to understand the different components in the experiment and their effects on the particle beam, a few concepts will be reviewed. Such concepts include the makeup of atoms, electron orbitals with respect to ionization energy, photo-ionization of atoms due to laser excitation, and magnetic field interactions with charged particles, particularly in reference to steering, focusing, and Lorentz Force Stripping.

Beginning in 1913, Niels Bohr explained the energy relationship of an electron to the hydrogen atom's nucleus as follows [8]:

$$E_n = \frac{m_e e^4}{8\epsilon_0^2 h^2} \left(\frac{1}{n^2} \right) = - \left(\frac{E_0}{n^2} \right) \quad (\text{Eq.3.1})$$

for any positive integer value for n where h is Plank's constant, e is the electron charge, ϵ_0 is the permittivity of a vacuum, m_e is the mass of the electron, and E_0 is defined as [8]:

$$E_0 = \frac{m_e e^4}{8\epsilon_0^2 h^2} = 13.595 \text{ eV} \quad (\text{Eq.3.2})$$

So, from Eq. 3.1, we find that an electron can have any of a series of negative energies, which will place it in a corresponding orbital, also referred to as states or levels, about the nucleus. The most negative energy state corresponds to the n=1 state or the ground state of the electron, which most naturally occurs unless additional energy is absorbed by the atom which raises the atom to a higher state. Below is a diagram of the atomic states related to the electron orbitals for the hydrogen atom.

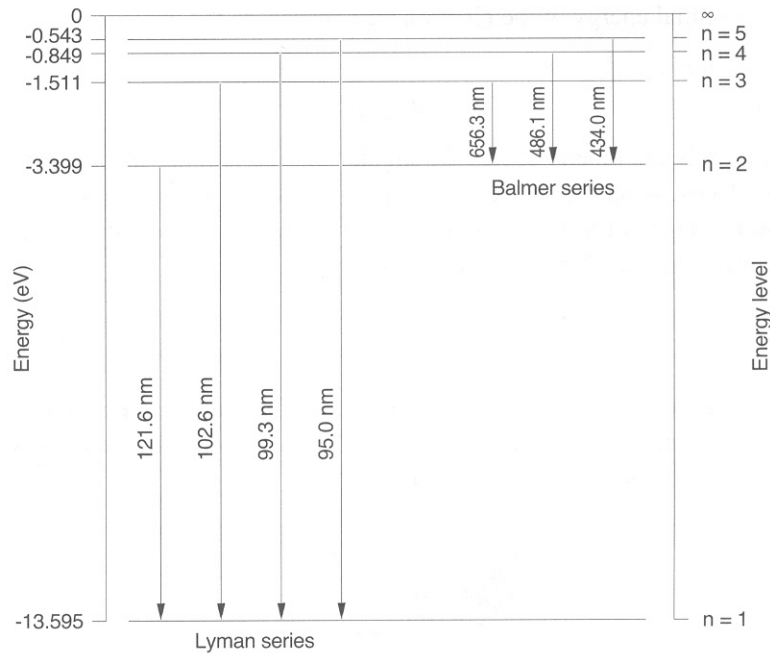


Figure 3-1 - Energy-level diagram of atomic hydrogen showing the first five energy levels and some of the radiative transitions between those levels (reproduced from [8])

The H^- ion and H^0 atom may be ionized through the Lorentz stripping process: a static magnetic field is transformed into a strong electric field in the rest frame of the particles. This field may be strong enough to “strip” an electron from the H^- ion or H^0 atom. Let’s begin by defining a few relationships and then we will elaborate on the consequences of the relationships. From the following equation:

$$E = \beta\gamma cB \quad [7] \quad (\text{Eq. 3.3})$$

we have a relation of the Electric Field, E , in the rest frame, and the magnetic field, B , where $\beta = v/c$, $\gamma = (1 - \beta^2)^{-1/2}$, and v and c are the velocities of the H^-

ion and light, respectively. The lifetime of the H^- ion in the presence of a magnetic field is given by the following relation:

$$\tau = \left(\frac{A_1}{E}\right) \exp\left(\frac{A_2}{E}\right) [7] \quad (\text{Eq. 3.4})$$

where A_1 and A_2 are constants whose values given in Sherk [9] and Jason et al [10] as, $A_1 = 2.47 \times 10^{-6} \text{ Vs/m}$ ($\pm 4\%$) and $A_2 = 4.47 \times 10^9 \text{ V/m}$ ($\pm 0.25\%$). This means, that for a given velocity of particles, there is a certain electric field felt by the particle beam as defined by the magnetic field applied. Furthermore, the strength of electric field determines the lifetime of an atom and as the electric field gets stronger, the lifetime gets shorter. H^0 atoms see fields just like the H^- ions, but the field strength required to achieve the same lifetime experienced by the H^- ions is about 40 T at the $n=1$ state for H^0 . However the $n=3$ state for H^0 looks very similar to the $n=1$ state for H^- , as depicted in Fig.3-2, which implies that the $n=3$ state for H^0 would be stripped in a 2T field in much the same fashion as the H^- ion was stripped.

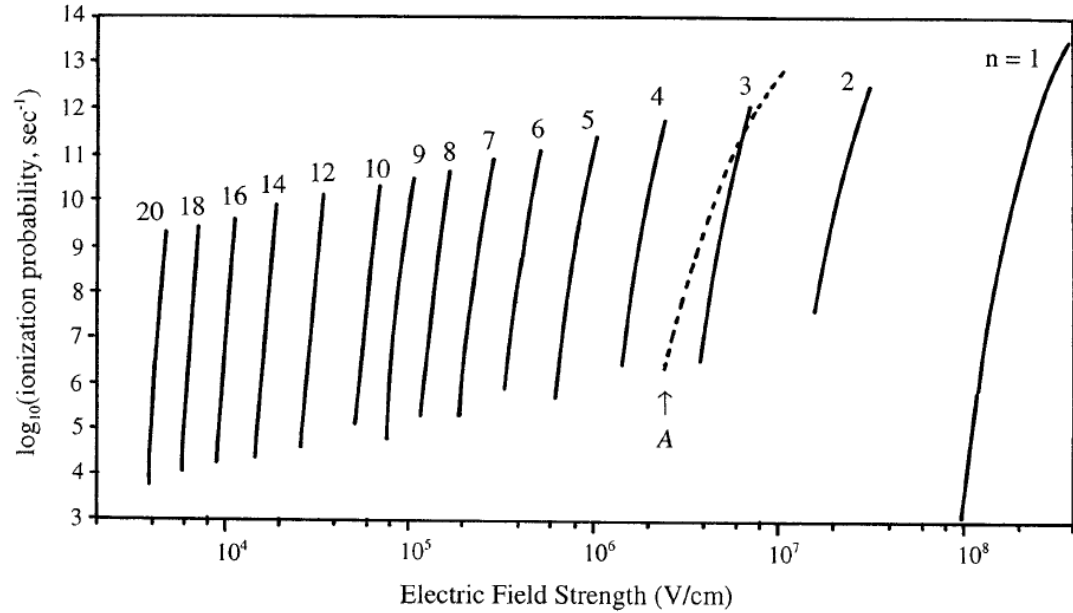


Figure 3-2 - Probability of Lorentz stripping for an H^+ ion and excited states of an H^0 atom. “ n ” is the principal quantum number of an H^0 atom. “ A ” indicates the probability of field dissociation for an H^+ ion. (reproduced from [7])

3.2. Photo-excitation

As stated in the previous section, there are varying levels of energies that electrons can occupy, and the higher levels can be easily achieved by adding energy by way of a light or heat source; one such light source that is commonly used is a laser. To find the wavelength of the laser needed to excite the electron to the $n=3$ state, we can employ Einstein’s relationship of energy and frequency, $E = h\nu$, and from Maxwell’s wave equation, $\lambda\nu = c$, we get a relationship which looks like [8]:

$$\lambda = \frac{hc}{E_1} = 91.4nm \quad (\text{Eq. 3.5})$$

This suggests that if we have a source of light with wavelength of 91.4 nm and it is absorbed by the atom, we can ionize the atom. The process by which photons of sufficiently short wavelength or shorter is absorbed by an atom to excite an electron to an infinite energy level or to excite the electron to an infinitely large distance (i.e. to ionize the atom) leaving a positively charged atom, is known as photo-ionization. Photo-excitation, however, is the process of introducing a light source of the wavelength that corresponds to the exact energy state desired without ionizing the atom.

We know that the relation of laser wavelength, λ_0 , in the H^0 atom rest frame to the wavelength, λ , in the laboratory frame is as follows:

$$\lambda_0 = \frac{\lambda}{\gamma(1 + \beta \cos \alpha)} \quad [11] \quad (\text{Eq. 3.6})$$

where α is the angle of incidence between the laser and the H^0 beam in the laboratory frame, $\beta = v/c$ (which is roughly .855 for a proton with kinetic energy of 870 MeV and .875 for a 1 GeV proton), and $\gamma = \sqrt{\frac{1}{1 - \beta^2}}$ (roughly 1.93 for 870 MeV proton and 2.066 for 1 GeV proton). Similarly, we can write:

$$\nu_0 = \nu\gamma(1 + \beta \cos \alpha) \quad (\text{Eq.3.7})$$

for the laser frequency

$$W_0 = W\gamma^2(1 + \beta \cos \alpha)^2 \quad (\text{Eq.3.8})$$

for the laser energy density, where W is the laboratory frame laser energy density (J/mm^2) and

$$\tan \alpha_0 = \frac{\sin \alpha}{\gamma(\cos \alpha + \beta)} \quad (\text{Eq. 3.9})$$

for the angle of incidence in the reference frame of the H^0 . The Doppler shift of the laser frequency is given by:

$$\Delta \nu_0^D = \nu_0 \beta \left(\frac{\Delta p}{p} \right) \quad (\text{Eq. 3.10})$$

for a particle with momentum error $(\Delta p / p)$. Usually, the momentum spread is $\sim .001$, so $\Delta \nu_0^D \approx 2.7 \times 10^{12} \text{ sec}^{-1}$. With the knowledge that the ionization energy of an electron from H^0 in the $n=3$ state is 12.10 eV, then we can calculate $\lambda_0 = c / \nu_0 = 102.6 \text{ nm}$, which is the wavelength needed to induce an excitation from the ground state to the $n=3$ upper state. The power density is given by:

$$Q_0 = cW_0 \quad (\text{Eq. 3.11})$$

and the power required by the laser is given by

$$Q_{lab} = Q_0 \left(\frac{\Delta \nu_0^D}{V_R} \right) d \quad [7] \quad (\text{Eq. 3.12})$$

where d is the duty factor of the laser which can be equivalent to the H^0 duty factor, and V_R is the frequency of the oscillations of particles between two quantum-energy states, known as Rabi oscillations, and is on the order of 10^9 .

The Rabi frequency is the angular frequency of Rabi oscillations which is defined as:

$$V_R = 2\pi N_R \quad (\text{Eq. 3.13})$$

where N_R is the number of Rabi cycles per second, and the generalized Rabi Frequency is given by:

$$\Omega_{i,j} = \sqrt{|\chi_{i,j}|^2 + \Delta^2} \quad (\text{Eq. 3.14})$$

where

$$\chi_{i,j} = \frac{\vec{d}_{i,j} \cdot \vec{E}_0}{\hbar} \quad (\text{Eq. 3.15})$$

$\Delta = \omega_{\text{light}} - \omega_{\text{transition}}$ and $\vec{d}_{i,j}$ is the transition dipole moment.

A simplified laser power formula is described by V. Danilov, et al, [4] which assumes an elliptical beam with constant density, a vertical size of Δ_y , which is taken to be slightly higher than the H_0 beam size of 1.8 mm (see Table 3.1) equating to 1.9 mm.

Kinetic energy (GeV)	1.0
H, V rms emittance (π mm mrad)	0.26
β_x, β_y (m)	10.4, 12.1
Horizontal, vertical beam sizes (mm)	1.6, 1.8
Horizontal, vertical angular divergences (mrad)	0.16, 0.15
Relative rms energy spread without momentum painting	0.3×10^{-3}
Relative energy spread with momentum painting	$\pm 4.0 \times 10^{-3}$

Table 3.1 - SNS parameters at the laser, particle beam interaction region (reproduced from [4]).

Additionally, we assume the total area of the laser beam is

$S = T\gamma c 2\Delta_y \times \sin(\alpha)\pi / 4 \approx 0.84 \text{ cm}^2$. Given these parameters, we can present the peak power is [12]:

$$P_{peak} = \frac{\ln(1/\delta)\hbar^2 \varepsilon_0 c^2 \kappa \omega_0 \sin \alpha \Delta}{2\mu_{1n}^2 \gamma (1 + \beta \cos \alpha)^2} \quad (\text{Eq. 3.16})$$

where $\delta \ll 1$ is the ratio of unexcited to excited atoms, which happens to be $\delta \approx 0.0067$ in this case, ω_0 is the laser frequency in the rest frame of the atom, and $\mu_{13} = -\int d^3 r u_1^*(\vec{r}) e z u_3(\vec{r}) = (3^3 e a_0 / 2^6 \sqrt{2})$, to represent the transition between states one and three. The probability of excitation of these particles to the n=3 state is depicted in Fig. 3-3, below.

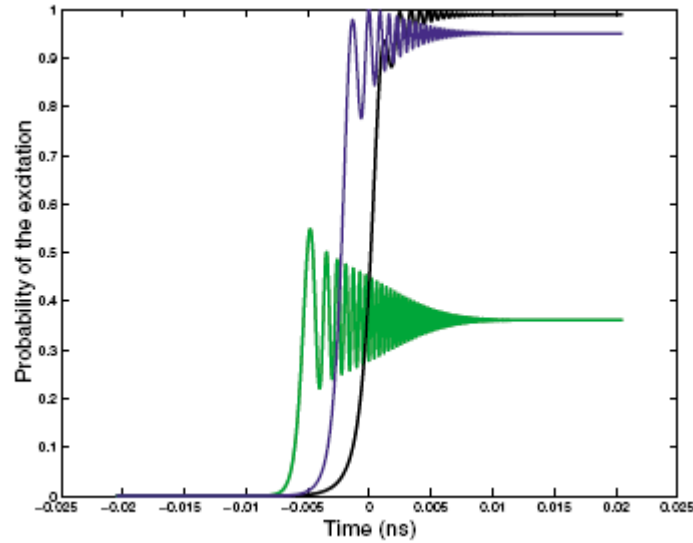


Figure 3-3 – Probability of the n=3 excitation versus time for reference energy particle (black line), the particle with the relative energy deviation 0.00025 (blue line), and 0.00075 (green line) (reproduced from [4])

3.3. Doppler Shift and Doppler Broadening

One of the major obstacles that needs to be overcome when setting up this experiment is to solve the problem of Doppler Shift and Doppler broadening. Characteristic frequencies, more commonly expressed in terms of wavelength, are possessed by radiating atoms. When a particle is accelerated, the kinetic energy increases due to the increased velocity. In the laboratory frame, an observer watching the particle approach sees a blue shift (or Doppler Shift) from the characteristic frequency. Because the H⁻ beam has a finite momentum spread, there is a Doppler broadening associated with the wavelength of the laser in the H⁻ beam rest frame. This broadening of the natural emission line width is largely a quantum mechanical phenomenon that is a direct result of radiating transition between two energy levels where the energy relation to the wavelength is simply:

$$E = \hbar\omega \quad (\text{Eq. 3.17})$$

By extension we can say:

$$\nabla E = \hbar\nabla\omega \quad (\text{Eq. 3.18})$$

One can see from equation 3.18 that the energy spread relates to a frequency spread. This poses a problem as a coherent laser of a very narrow frequency spread can only excite a certain percentage of the H⁻ beam that corresponds to a very narrow energy spread. As we will see, there is an ingenious method which counteracts the Doppler Shift and broadening seen by the ion beam.

3.4. Experimental Approach

As noted in earlier sections of this paper, by using a diverging laser beam at the injection region, we get a setup that looks much like the figure seen below:

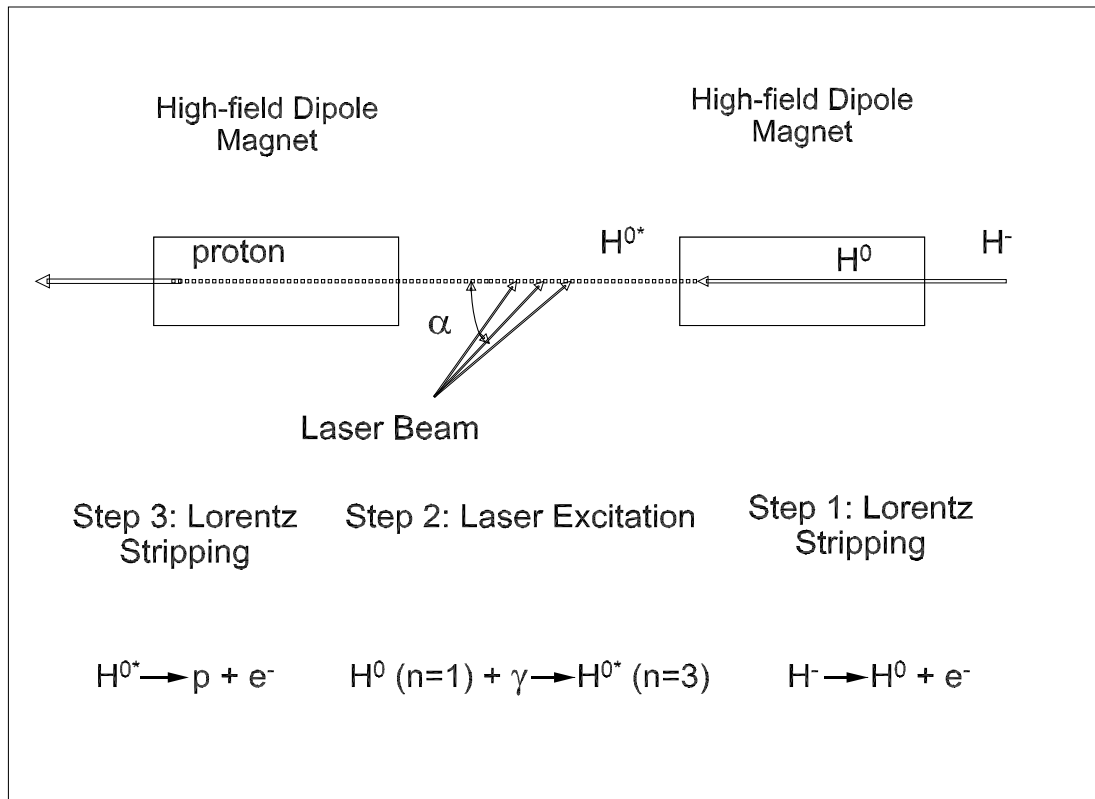


Figure 3-4 - Illustration of experimental setup (reproduced from [11]).

The H^0 beam inherits the frequency spread of the H^- counterpart (usually on the order of 10^{-4}). Since each atom has its own excitation energy, and the relative spread in frequencies is approximately equal to the energy spread (which in turn is proportional to the momentum spread), a coherent beam with an inherently small frequency spread would only excite a small portion of the beam for the third stage of stripping. Therefore, a diverging laser beam which yields slightly different angles of incidence for each individual atom, as seen in Fig. 3-4, is the

key to being able to strip the entire beam (Eq. 3.6). This strategy of matching the laser angle of incidence to the beam average energy and then introducing a divergence to the laser answers both quandaries of how to deal with Doppler Shift and broadening.

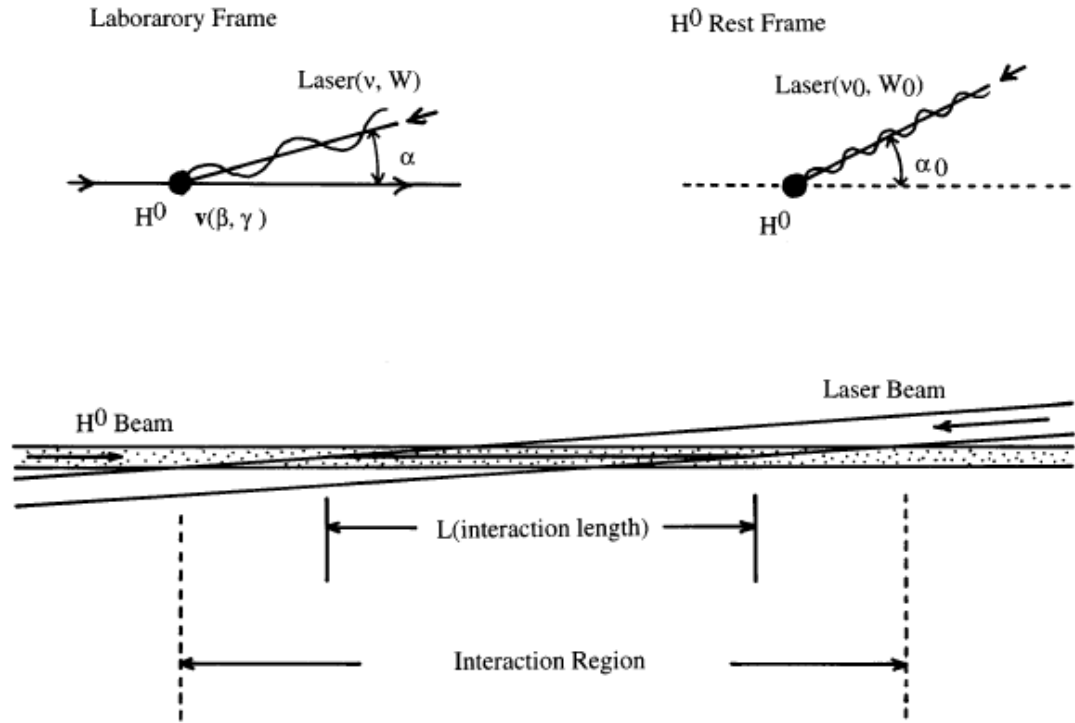


Figure 3-5 - Colliding system of an H^0 atom beam and a laser beam. Variables in the H^0 rest frame are shown in the upper right and those in the laboratory frame are shown in the upper left (reproduced from [7]).

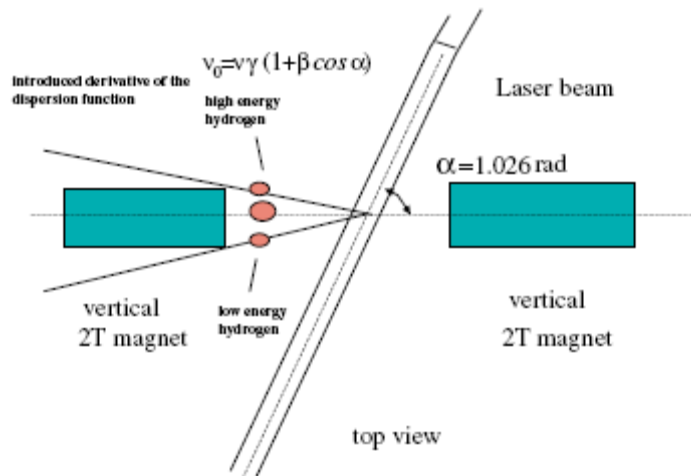


Figure 3-6 - (Color) Interaction region setup for the minimization of the Doppler broadening. Total length of the region is about 60 cm. (reproduced from [4])

In the laboratory frame, the laser frequency is kept constant. In the rest frame of the particle beam, however, because of the Doppler shift effect on the incidence angle of the laser, the frequency of light decreases as the $\Delta\alpha$ increases. The result is a so-called “frequency sweep” as the hydrogen atom traverses the laser interaction region until resonant frequency is seen. In addition, this “sweep” can be made large enough that all particles will eventually cross the resonant frequency and excitation will occur.

3.5. Charged Particle Motion in a Uniform Magnetic Field

Magnetic fields are used almost exclusively in accelerator environments to steer as well as focus charged particle beams as desired. In accelerator physics, most beam dynamics are derived from interpretations of the Lorentz Force equation

$$F = q(E + v \times B) \quad (\text{Eq. 3.19})$$

where force \mathbf{F} , electric field \mathbf{E} , velocity \mathbf{v} , and magnetic field \mathbf{B} are all vector quantities. For magnetic fields, the Lorentz force is normal to the direction of beam propagation, therefore the equation simplifies to the scalar formula found in Eq. 3.20.

$$F = qvB = m \frac{v^2}{r} \Rightarrow r = \frac{mv}{qB} \quad (\text{Eq. 3.20})$$

Eq. 3.19 simplifies to Eq. 3.20 yielding the relation between force, mass m , scalar velocity v , and charge q , assuming zero E-field. Fig. 3-5 below shows the forces on a charged particle entering a magnetic field at a certain velocity, v , are orthogonal to the direction of propagation and orthogonal to the B-field; thus yielding a bending force in the transverse direction which can steer and, when the appropriate pole tip configuration is employed, can focus the charged particle beam.

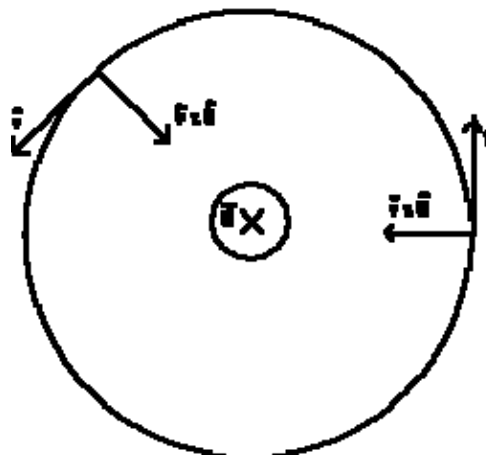


Figure 3-7 - Motion of a charged particle in a magnetic field (reproduced from [15])

In our experiment, we utilize another phenomenon which is readily observed from magnetic interactions with charged particles: Lorentz stripping. Lorentz stripping occurs when the H⁻ ion which enters the B-field experiences a Lorentz Force that affects the trajectory, but the ion itself starts to split up because the electron in the highest electron orbital is bent in a different direction because of its weak binding energy of 0.755 eV [16]. The other electron, the one in the lowest energy level, has a much higher ionization energy, and cannot be removed as easily. This is a quantum mechanical process which depends on the increased probability of the additional electron to tunnel through the potential well by manipulating the potential well in the rest frame of the H⁻ ion through the application of an electric field. This electric field can be obtained by taking the Lorentz transform of the B-field by:

$$E = \kappa' \beta \gamma B \quad (\text{Eq. 3.21})$$

where $\kappa' \simeq 0.3 \text{ GV/T-m}$. $E [\text{MV/cm}] = 3.197 p [\text{GeV}/c] B[\text{T}]$ for the H⁻ ion where p is the ion momentum in the laboratory frame [15]. For a 1 GeV H⁻ ion in a 1 T field, the electric field in the rest frame is $\sim 5.5 \text{ MV/cm}$.

Alternatively, we can describe this phenomenon classically, with respect to energy only, if we consider an electric potential, $V(r)$, as defined in [13] as:

$$V(r) = -r^{-1} - F_z \quad (\text{Eq. 3.22})$$

where F_z defines the z axis. $V(r)$ has a saddle point in the z axis whose value is:

$$V_{sp} = -2\sqrt{F} \quad (\text{Eq. 3.23})$$

In this saddle point view an ion is said to be stable if the energy, U , is less than V_{sp} , and ionized if U is greater than V_{sp} , yielding stable ions only when:

$$U \leq -2\sqrt{F} \quad (\text{Eq. 3.24})$$

Ignoring the Stark Effect, here, we can say $U = 1/2n^{*2}$, where n^* is the effective quantum number. We can further deduce from Eq. 3.24 that the probability of ionization is at a threshold field value of:

$$F_c = 1/16n^{*4} \quad (\text{Eq. 3.25})$$

Table 3-1 illustrates the nominal parameters for the experiment that is described in the next chapter. In this table, take special notice of the vertical and horizontal size of the laser beam and the ion beam. Both beams exhibit a much larger horizontal size compared to the vertical size, and the laser divergence is around 6-8 mrad, which supports the theoretical setup to mitigate the Doppler broadening effect.

Chapter 4

Experimental Setup

4.1. Facilities

The Spallation Neutron Source is an accelerator-based neutron source in Oak Ridge, Tennessee, USA, which was a collaborative effort from six different DOE facilities which include: Lawrence-Berkeley National Lab, Los Alamos National Lab, Jefferson National Lab, Brookhaven National Lab, Argonne National Lab, and Oak Ridge National Lab. At full power, SNS will provide the most intense pulsed neutron beams in the world for scientific research and industrial development, delivering 1.4 MW of proton beam to the mercury target. SNS consists of a Front End, Linac, which is comprised of a normal conducting and a super conducting accelerating cavity section, an accumulation ring, a mercury target and associated target hall for experiments, and two transport lines to and from the ring which contain beam diagnostic systems, beam manipulation sections, and include dumps for safety precautions.

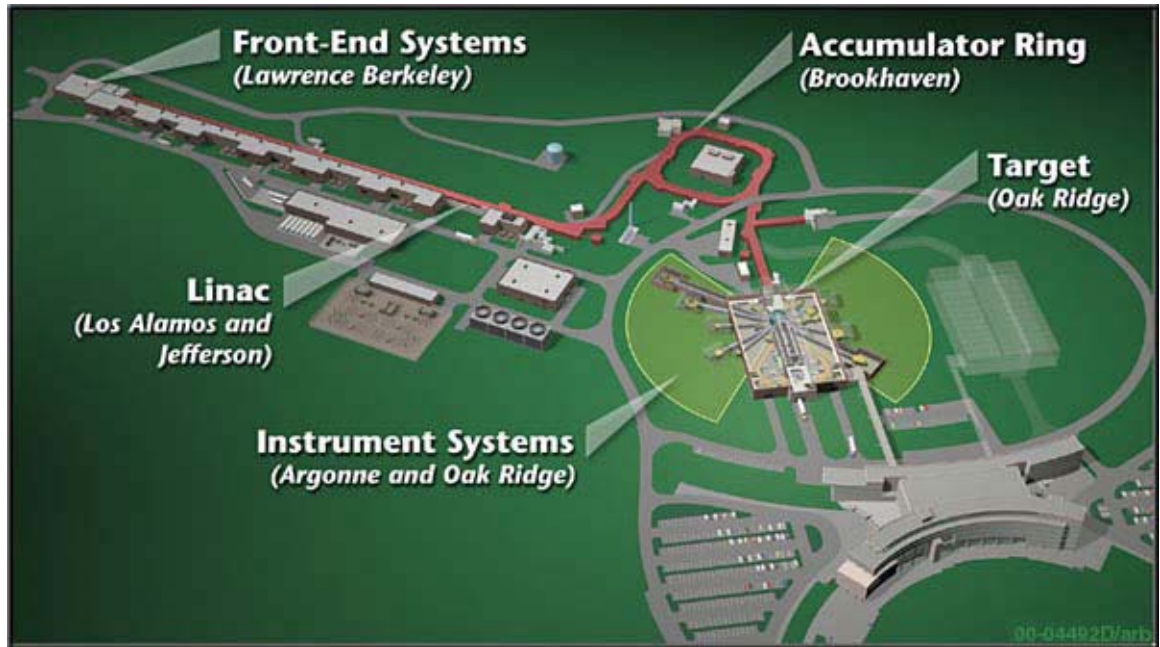


Figure 4-1 - Illustration of the SNS site. The acceleration begins at the Front-End Systems, is accelerated through the Linac, sent through the High Energy Beam Transport to the Accumulator Ring and then sent through the Ring to Target Beam Transport to hit the target.

4.2. Front-End and Linac

The SNS front-end system includes an ion source, beam formation and control hardware, and low-energy beam transport and acceleration systems. The ion source produces H⁻ ions that are formed in a cesium assisted plasma, and then extracted and steered through an electrostatic Low Energy Beam Transport (LEBT). The continuous beam extracted from the LEBT is formed into a pulsed beam and accelerated by a Radio-Frequency Quadrupole (RFQ) section to a design energy of 2.5 MeV. The beam is, then, transported in the Medium Energy Beam Transport (MEBT) which contains diagnostic functionality as well as beam matching functions. Both the accelerating and bunching cavities in the RFQ and MEBT operate at 402.5 MHz repetition rate and are designed for 1 ms beam at 60

Hz. The next section into which the beam is then injected is the Drift Tube Linac (DTL) which includes six accelerating cavities and is also operated at 402.5 MHz, accelerates the beam from 2.5 MeV to ~87 MeV. From there, the beam enters the Coupled Cavity Linac (CCL) which is the first of the 805 MHz operated cavities. By the time the beam leaves the CCL and gets injected into the Superconducting Cavity Linac (SCL), it has an energy of ~185 MeV. The SCL is constructed from two different module designs: the medium beta, designed for an average $\beta = 0.61$, and the high beta, designed for an average $\beta = 0.81$. The entire Linac combines to accelerate the beam to 1 GeV. The beam is, then, transported through the High Energy Beam Transport (HEBT) to the accumulator ring, and the beam current is increased through stacking, which is utilizing the opposite charges of the circulating and incoming beams to combine the two just before they pass through a charge exchange system, traditionally consisting of a carbon foil. Stacking is performed in an accumulation ring so as to achieve high currents and maintain the design emittance of the beam for that machine. Once the requested beam current is attained, the particle beam is kicked out through the extraction section in the Ring to the Ring to Target Beam Transport (RTBT), and delivered to the Target. If we were to turn off one critical device in the HEBT, nominally the first major bending dipole, we would be set up to go straight into the Linac Dump, which is where the Laser Stripping experiment took place.

4.3. Experimental Layout

The experiment consisted of two distinct aspects: the laser beam transport and the particle beam delivery system. As already described, the magnets needed for the experiment were placed in the beam line just before the Linac Dump in the SNS Linac, and the laser table which held the telescoping optics were arranged adjacent to and in the plane of the beamline. The laser employed was a frequency tripled Q-switched Nd:Yag (Continuum Powerlite 8030) laser capable of emitting a 13.7 MW laser beam at 355 nm in a 6 ns pulse. It turns out, however, that the power of the laser, or power delivered to the ion beam, was limited to ~ 10.5 MW as etching was observed on the vacuum windows attributed to the higher intensity laser beam. Our theory is that higher laser power at higher concentrations facilitates erosion of the molecular level of the window causing scratches in this surface which are deep enough to cause a vacuum leak at these points.

At this wavelength, Eq. 3.1 requires an angle of incidence between the laser and the 1 GeV particle beam $\alpha = 38.8^\circ$ to achieve 102.6 nm in the hydrogen atom rest frame. The interaction region, which was located between the dipoles, was designed with a specialized vacuum chamber which had a flange (see Fig. 4-2) on the laser side with four vacuum windows designed to accommodate four discrete laser angles of incidence. This was done to be flexible enough to perform the experiment at varying beam energies which proved advantageous because the ion beam from the Linac had a lower energy than the expected 1 GeV. In fact, our experiments were done at energies around 870 MeV with the lowest incident

angle of 20 degrees, as compared to the initial design angle of 40 degrees for a 1 GeV beam.

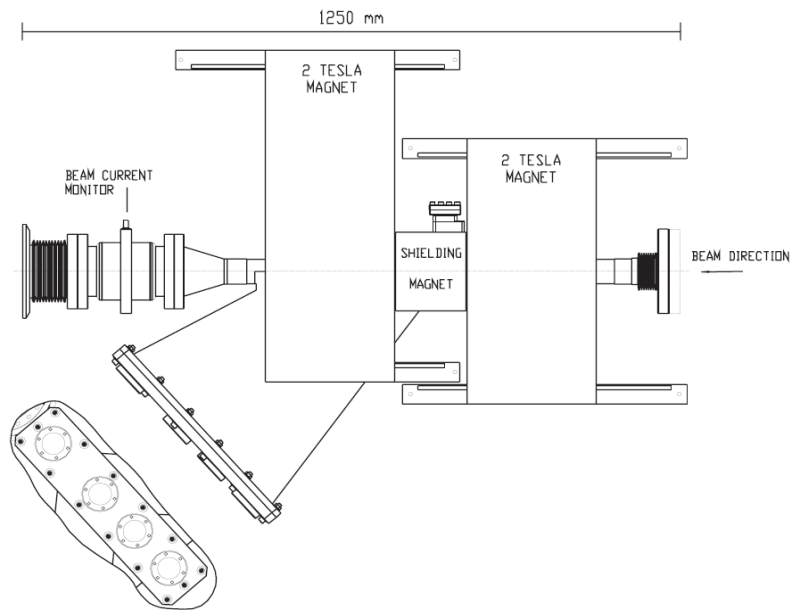


Figure 4-2-Stripping assembly layout (top view). One can see two strong 2T magnets with mechanical supports, the vacuum chamber with ceramic break and toroid on the left side of the assembly, and the laser window flange; top view at the bottom of the figure (reproduced from [11]).

Badker Institute of Nuclear Physics (located in Novosibirsk) manufactured the assembly in 2005 which consisted of three magnets: 1) The first magnet encountered by the beam was a 2T magnet for electron detachment; 2) The second was a small shielding magnet in the interaction region which reduced the effect of stray fields from the two adjacent magnets in this region; 3) The third was a second 2T magnet for the last stripping stage which is modified in order to accommodate the specialized flange.

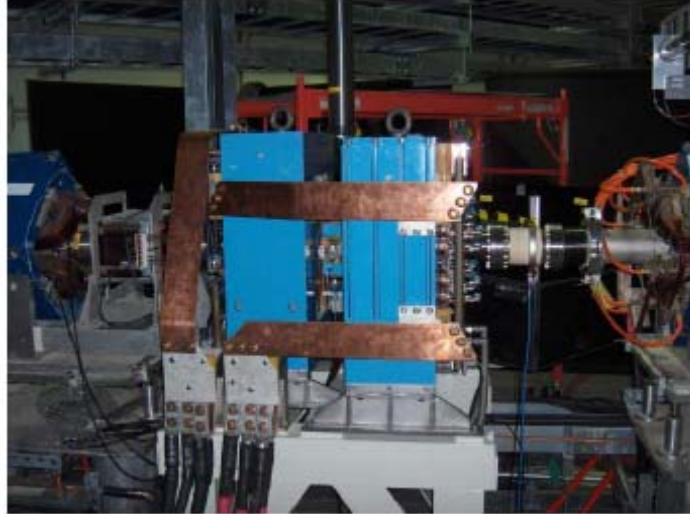


Figure 4-3 - Physical setup in the tunnel of the two magnets (the two blue objects) and the interaction region (reproduced from [12])

4.4. Ion Beam Optics, Laser Beam Layout, and Optics of Laser

From 3.16, we know the laser power required for stripping an 870 MeV beam is ~ 10 MW. In order to match the requirements needed to compensate for Doppler Shifting, it was necessary to place a set of telescoping optics in to make the laser beam wide, horizontally, and narrow, vertically. Figures 4-3, 4-4, and 4-5 show the setup and design of the laser optics, and Figure 4-6 shows what the laser beam looked like after telescoping and in the interaction region with the particle beam.

The controls for the telescoping optics were few, but enough to accomplish the goal of making the horizontally wide and vertically narrow laser beam at the interaction region. The laser beam comes into the table transversely uniform before it encounters the telescoping optics which includes a convex lens,

a concave horizontally focusing lens and a concave vertically focusing lens (see Fig. 4-5). All of the telescoping optics are on translation stages connected to stepping motors for fine remote control after the coarse local tuning is achieved. Laser power is verified locally during every tune-up as well as alignment and size verification and adjustments as seen in Fig. 4.6. The screens seen inserted in Fig. 4-6 are a temporary visual aid and are removed once the tune-up is complete. Once the laser enters the vacuum chamber its path is determined from the optics, which is intended to direct the shaped laser to the laser absorber which is on the opposite side of the vacuum chamber relative to the window side.

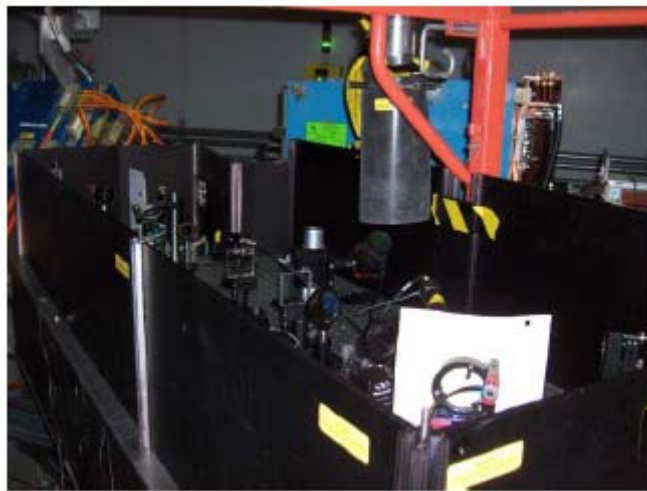
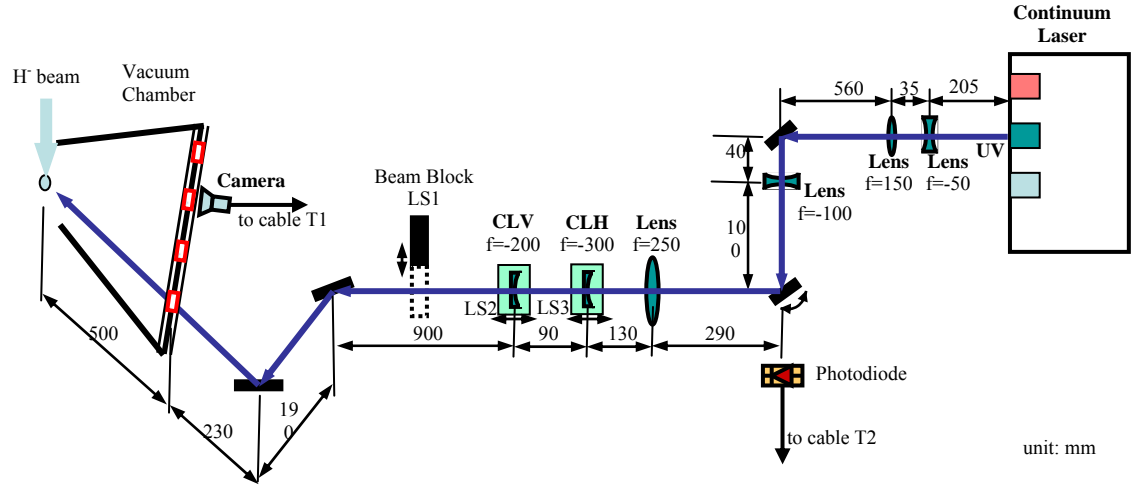


Figure 4-4 - Laser table and optics view from the top (reproduced from [12])

Optics Setup



Estimated beam parameters at the interaction point:

$2w_0 = 3.9 \text{ mm}$, $2\theta_0 = -8.0 \text{ mrad}$, $2w_1 = 4.8 \text{ mm}$, $2\theta_1 = -4.3 \text{ mrad}$.

Linear stage #1: beam block (insert position)
 Cables: #1918 (flash lamp trigger in), #1919 (Q-switch trigger in), #T1 (camera), #T2 (photodiode)

Fig. 4-5 - The laser optics setup on the table in Fig. 4-4

Laser Beam Images at Different Positions

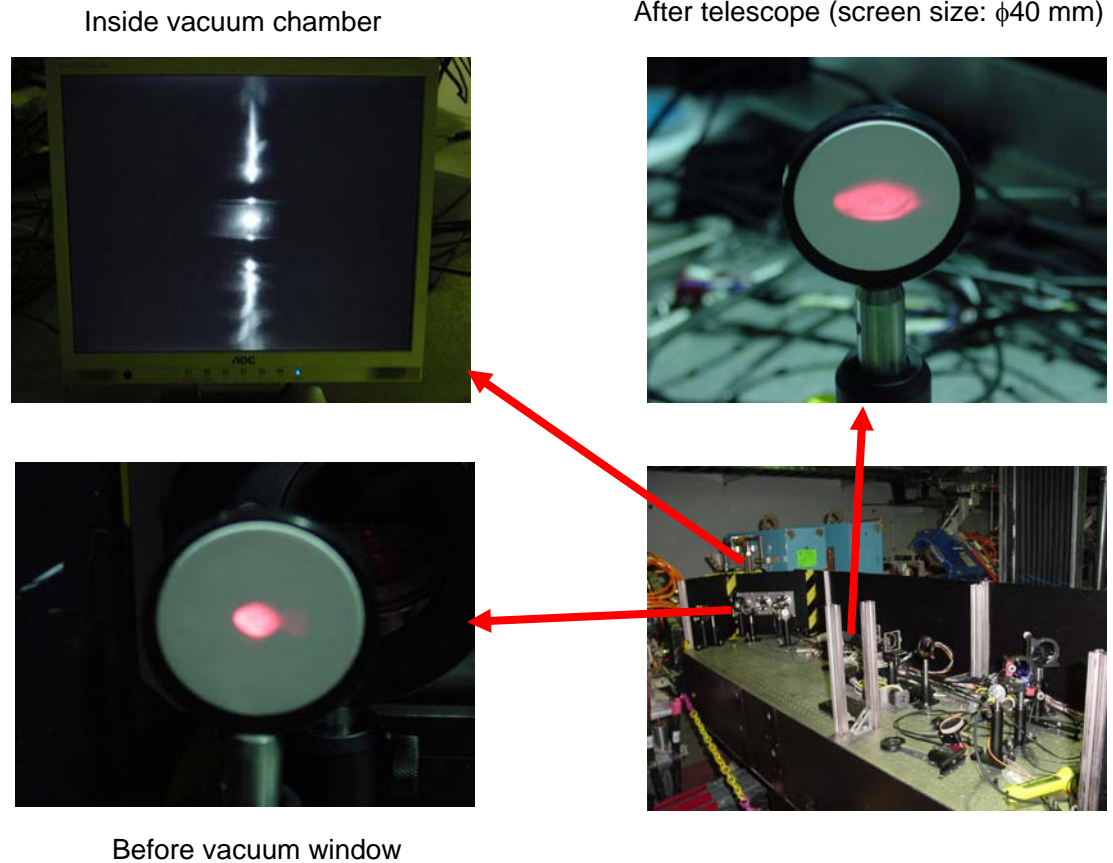


Fig. 4-6 - Figure of laser beam profiles at different points of the optical layout. We wanted for the beam to look flatter than the top right at the window, but that condition contributed to the window damage.

Other optic controls included on the laser table are deflecting mirrors which are adjusted during the tune-up and are afterward fixed for the remainder of the run. In addition, there is a beam block which can be remotely inserted to remove the laser from the interaction region for various reasons. It was common practice to turn on the laser after a tune-up, and then control the beam through the use of this beam block along with one other beam stop upstream from the table. This was done for two reasons: 1) the laser power fluctuated until the power supply reached thermal equilibrium which could take up to ten minutes; 2) the

laser was energized and de-energized locally making the ability to easily control the laser difficult as most of the data was taken from a remote locale.

Additionally, the Ion Beam is flattened at the interaction region to maximize the number of interactions and minimize the average laser power needed to excite the remaining electron. One can visualize from the β - function for the Ion Beam at the interaction, as shown in Figure 4-7, that the beam is, in fact, wide, horizontally, and narrow, vertically. In addition, the space-charge forces act to form the beam in a circular and uniform fashion just as it hits the vacuum window on the Linac Dump. The design of the Linac Dump requires that the beam be uniform on the window because, otherwise, the window may be compromised or the plates, of which the dump is made up, may be damaged or cracked as a result of the undo localized thermal stress resulting from a non-uniform beam bombarding the Linac Dump assembly.

As already stated, Fig. 4-7 shows the results of linear optics design that meets the constraints of the interaction region, and the constraints on the Linac Dump. In order to achieve this profile, we introduce perturbations to the uniform beam size at a point that is around 25 m upstream of the interaction region through the use of quadrupole magnets. This may seem a bit extreme or unnecessary to begin this bump early, but this is absolutely crucial as physical constraints impede the degrees of freedom available to achieve the goal. One obstacle to overcome is the small effect that the magnets have on the beam inherent to the energy of the particle beam. Logically, one must begin further upstream to shape the beam for the desired size as this provides an early

perturbation so that the steering required is within the range of the magnets' potential B-fields. In addition, the quadrupole magnets are mostly connected in groups to common power supplies. Nominally, there exists one power supply controlling the only two horizontally focusing magnets in the Linac dump, and only three power supplies to control the four vertically focusing magnets in the same region. These two main impediments work together to make the number of solutions to the constraint issues to be small. To compound the hurdles, one must vary both horizontal and vertically focusing quadrupole magnets, simultaneously, because there is a coupling between the horizontal and vertical beta functions. The Methodical Accelerator Design (MAD) program sponsored by Conseil European pour la recherche Nucleaire (CERN) was useful to achieve these solutions, and ultimately, the optics design shown in Fig. 4-7 was translated from the theoretical and attained in the practice.

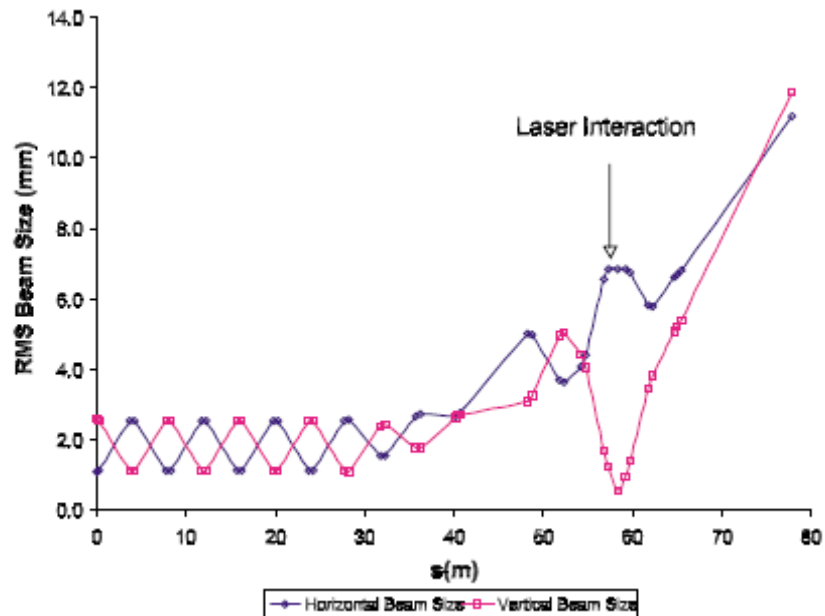


Figure 4-7 - Proposed β - function at the interaction region. It is clear from this picture that the beam is wide, horizontally, and very narrow, vertically. (reproduced from [4])

Chapter 5

Results of Experiment

Results from the March of 2006 experimental period, shown in V. Danilov (et.al) [12], record our first stripping results of 50 % (given by the ratio of the stripped proton current to the incoming ion current). Higher efficiency was not achieved during this period, however, as the vacuum windows on the flange had begun to leak as a result of structural weakening caused by etching of the vacuum window discussed in the last chapter. Subsequent experimental runs yielded as much as 93% (assuming the higher end of the error). The results presented here have been published in V. Danilov (et. al) [12].

Ordinarily, the stripped proton current and the incoming ion current could be obtained with a Fast Transformer (a Bergoz FCT-178) located downstream of the third magnet (as seen in Figure 4-4), which is depicted in Figure 5-1. The short laser pulse, however, strips only a 6 ns (FWHM) slice of a much wider (~ 700 ns) incoming ion beam pulse, and the measuring system has a bandwidth designed to measure the 700 ns pulse, but insufficient to accurately measure the 6 ns stripped pulse. In fact, the dispersion of the signal due to the cable length of 85 m makes the signal amplitude degrade and the width of the signal increase; an effect which was corrected by using the transfer function of the cable to restore the signal of the stripped beam. After all of the parameters were factored in, including a measured 5% pulse to pulse jitter of the ion beam, we estimated that we had a $\pm 10\%$ error on our stripping efficiency calculation, and the highest

calculated stripping yield was ~90%. This 90% stripping efficiency was achieved through the reduction of the vertical ion beam size at the interaction region to around 0.6 mm. Further optimization could have been achieved by increasing the power density of the laser at the interaction region, but a more focused laser power deposited on the vacuum windows proved to be the agent which caused the breakdown.

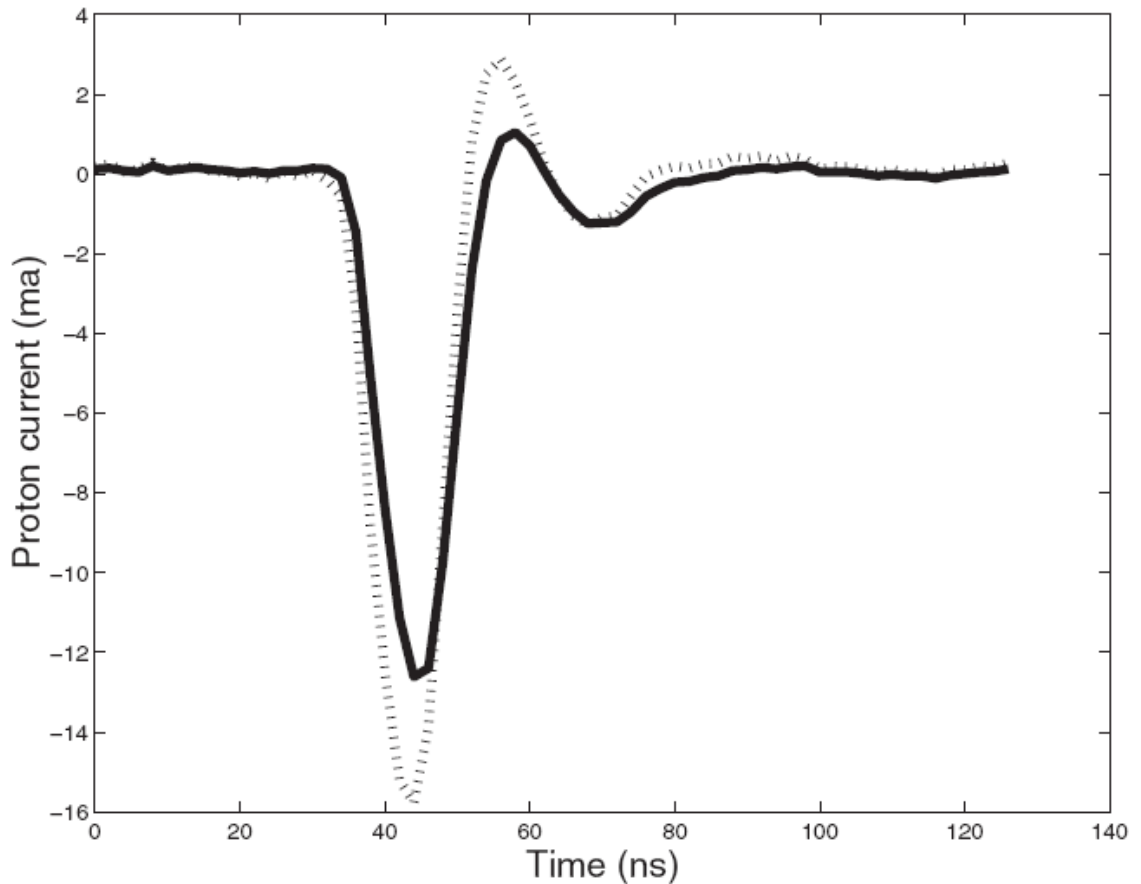


Figure 5-1 - Proton Signal from the stripped H- protons as recorded by digital oscilloscope (solid line), and restored original signal from beam current monitor (dashed line) (reproduced from [11]).

A more quantitative prediction of the stripping efficiency was desired which took into account the full 6D distribution of the ion beam and the real profile of the laser beam. Numerical simulations based on our theory of stripping

were performed, allowing us to compare our theoretical understanding to the experimental observations, and to form an efficiency study versus some of the laser and the ion beam parameters [11].

Since the most obvious parameter which has the largest potential for uncertainty is the vertical ion beam size, we needed to ensure that the vertical beam size was accurately estimated. We measured the twiss parameters and the emittance of the ion beam at the interaction region by varying upstream quadrupole magnet strengths and performing a wire scan with a device (one scan is depicted in Fig. 5-2) located about 2 m downstream from the interaction region. After measuring the twiss parameters, we can use our model to project back to the interaction region to achieve both vertical and horizontal beam sizes at that point. Restored ion beam sizes vary from 0.5 mm to 1.0 mm, which was enhanced by the stripping size s caused by the 2 T stripping magnet; the new ion beam size after the stripping process is transformed to $\sqrt{s^2 + (0.25)^2}$ mm. Therefore, we were led to the conclusion that the vertical beam size was a Gaussian distribution with a sigma of between 0.55 mm – 1.05 mm.

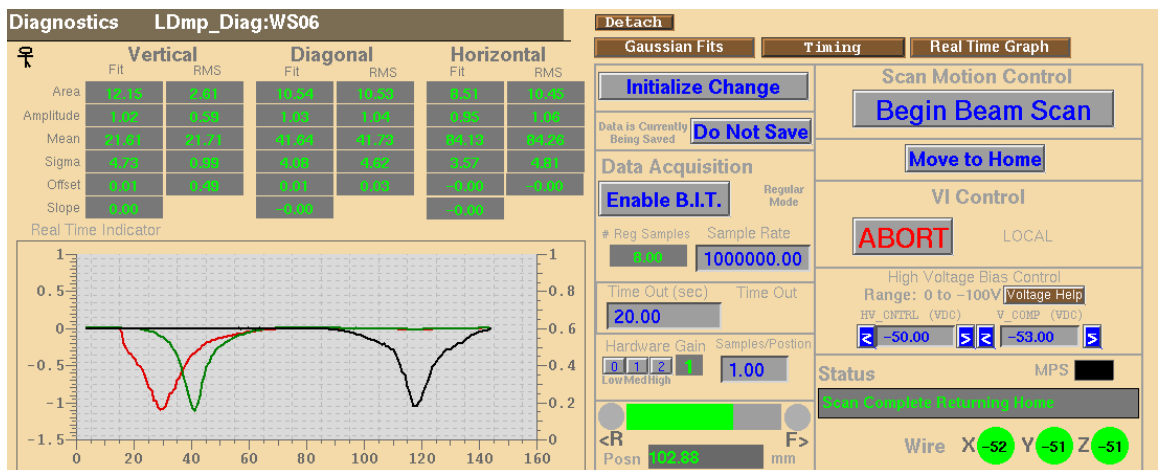


Figure 5-2 - This image is taken just before the dump where the restoring, space-charge forces form the ion beam into more of a circular shape at the dump.

The beam measurements available to us are incapable of measuring beam distribution accurately so we cannot say explicitly that the ion beam distribution is Gaussian. In addition, changing laser energy definitely changes the dynamics of the laser which can manifest in density variations including but not limited to spatial ring development in the profile which indicates higher order modes being propagated. As the model uses a Gaussian distribution of particles and makes some other simplifying assumptions related to the laser modes, the data measured is likely to vary when these assumptions break down. Energy dependence is also taken into account in the model, while our measurement of this variable is limited, which can lead to further deviations. With this information in mind and with the knowledge that the results were meant to be more quantitative and less qualitative, we can look at the experimental data.

Experimental data shown in Fig. 5-3 (depicted by points with error bars), is shown alongside the calculated curves for the ion beam sizes of 0.55 mm and 1.05 mm, respectively. These data were taken with a peak laser power of 6.25 MW at 2 mm FWHM vertical laser beam size.

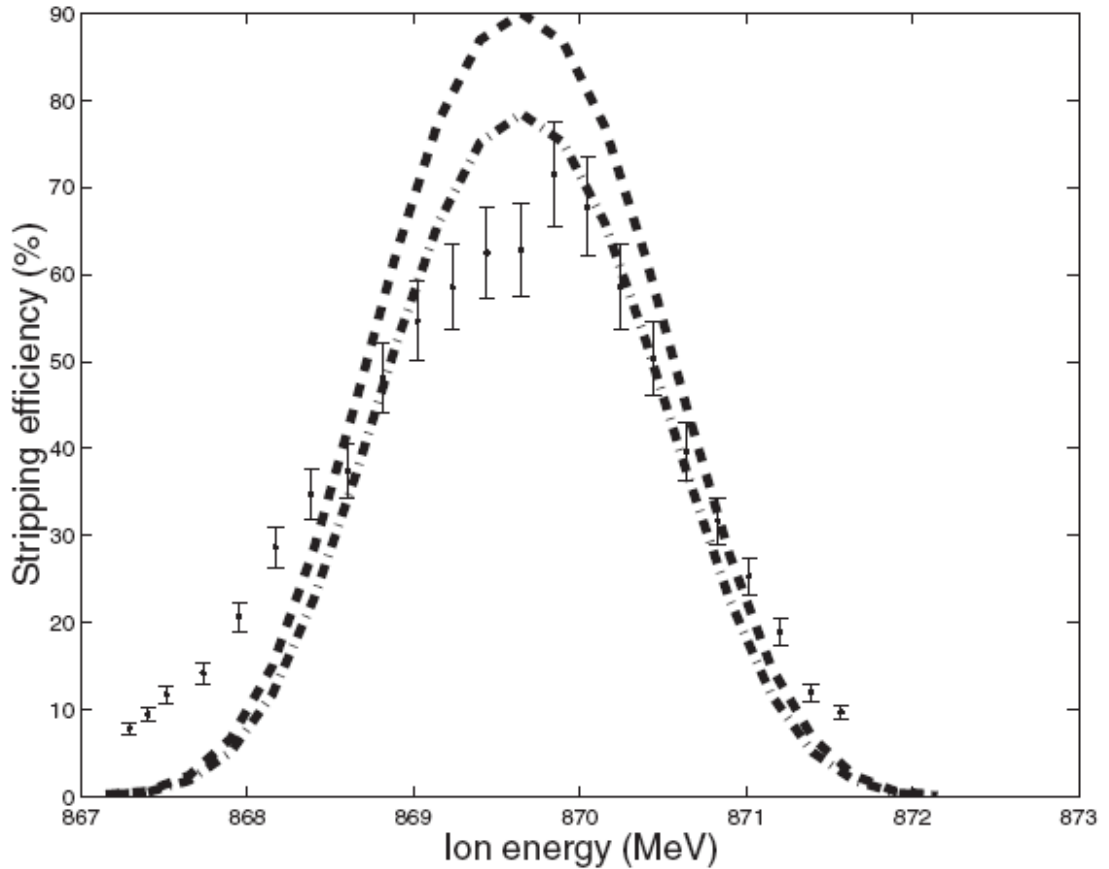


Fig 5-3 - Experimental data (error bars) 0.55 mm vertical beam size (dashed line), and 1.05 mm vertical beam size (dash-dotted line) (reproduced from [11]).

One can observe that the measured data matches neither the predicted maximum stripping efficiency nor the calculated optimal energy at which the maximum stripping occurs, exactly. This phenomenon is most likely due to the ion beam distribution containing tails which skew the data from the predicted outcome. Similarly, we performed a check of the stripping efficiency vs. the laser beam peak power in Fig. 5-4. The significant deviation of the measured values to the predicted values for low peak power values can be attributed to the fact that laser beam quality degrades at lower pulse energies in addition to the beam area increasing proportionally with the power decrease.

An additional measurement that was attempted during the October 2006 experiment period was to compare the stripping efficiencies of two different laser bandwidths. The first bandwidth, which was the narrower, (on the order of 10^{-7} relative width) we used for the experiment described above, and the second was a broader spectrum by a factor of about 300 achieved by turning off the seed laser. The results of the stripping efficiency of the two bandwidths showed dependence of stripping vs. energy on the same order as was observed in the experimental data, but the stripping efficiency dropped 25% for the unseeded laser mode (from 85% to 60%). In the process of going from one laser mode to the next the Linac was turned off. Some variables could have been the ion beam vertical size being adversely affected by hysteresis in magnets in the region, for instance, or other ion beam parameters being changed or varying. We already know that the pulse to pulse variations in the ion beam currents were about 5% during the seeded experimentation period. Therefore, it is likely that the beam conditions varied from run to run.

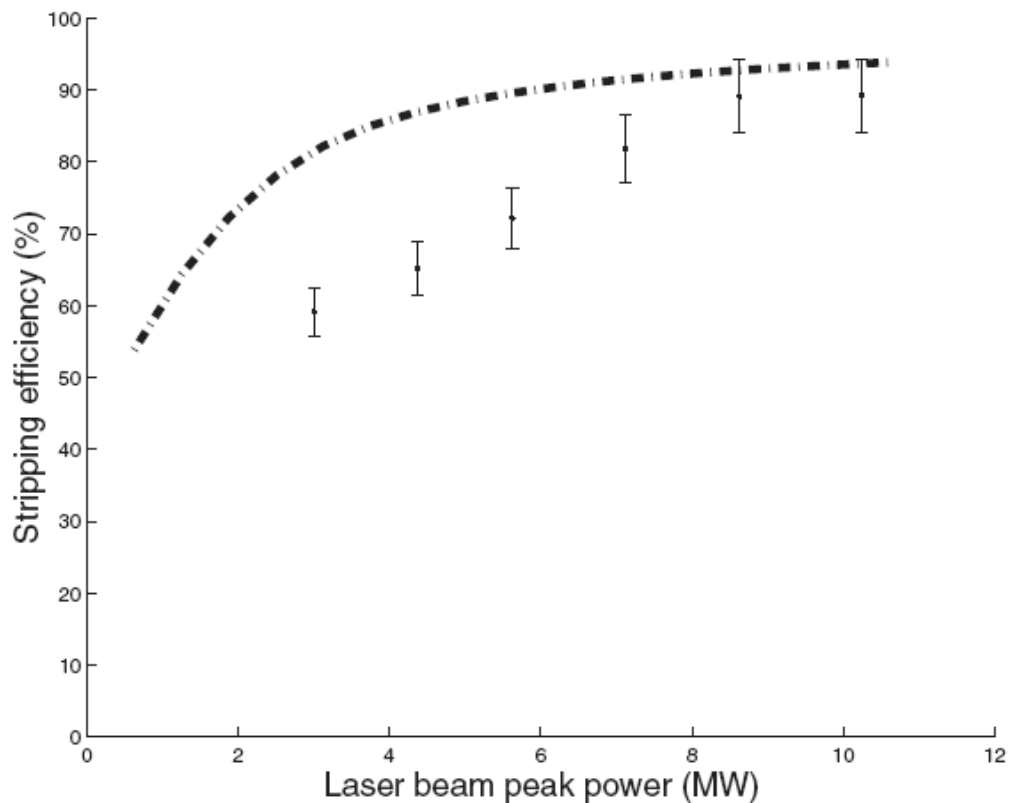


Figure 5-4 - Measured (dots with error bars), and calculated (dashed line) stripping efficiencies versus laser pulse peak power. The calculated efficiency reaches 99% for 20 MW laser peak power (reproduced from [11]).

Our data shows that lasers with larger bandwidths can be used for stripping purposes, as well, as a 25% reduction in stripping efficiency corresponds to a factor of 2 reduction in laser beam power as seen in Fig. 5-4. We can attribute the relatively high stripping efficiency of the unseeded laser to the fact that, even though the spectrum increased by a factor of 300, the relative spread of the laser (3.5×10^{-5}) is smaller than the energy spread (on the order of 10^{-4}). We can say, then, that the Doppler spread from the laser beam divergence is greater than the frequency spread of the light caused by the unseeded laser's excited harmonics (i.e. the excitation process is still adiabatic).

Chapter 6

Conclusions & the Future of Laser Stripping at the SNS

Demonstration of short pulse stripping has been effectively shown to be a reality, but further demonstration of long pulse stripping is required to make laser stripping a reality for replacement of the foil stripping scheme. A plan is underway to install the next generation laser stripping experiment which will utilize a more powerful laser, manufactured by Continuum, with the use of a Fabry-Perot resonator (Fig. 5-1). The resonator is a pair of mirrors which create a channel through which the laser can interact with the ion beam multiple times. With more passes of the same laser beam the overall average power requirements of the seeded laser will be drastically reduced. In addition, such changes as matching the temporal profile of the laser light to the ion beam, and reduction of the vertical size of the ion beam, which requires less laser power, are steps that will enhance the stripping efficiency as well as lower the overall power requirements for the laser beam. We estimate, as mentioned above, that by matching the laser to the ion beam, i.e. 50 ps, 402.5 MHz repetition rate, and 6% duty cycle, we should be able to improve on the stripping efficiency. If we figure on 10 passes in the Fabry-Perot resonator we can say that the repetition rate for the laser can be 40.25 MHz, and we can configure the resonator so that the laser beam passes through the ion beam every 2.5 ns.

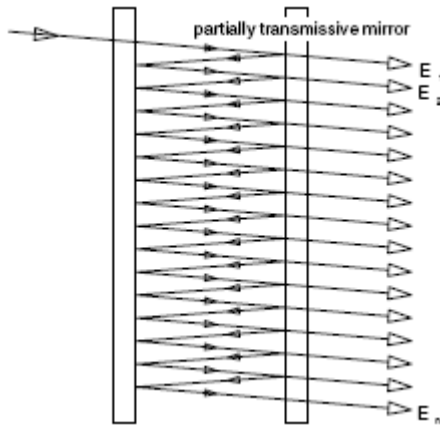


Figure 6-1 - A multipass interferometer originally proposed by A. Fabry and Ch. Perot in 1897 is still used in spectroscopy applications and laser resonators (although the applications use mainly curved mirrors) [17].

The optics should also be designed to minimize the small laser spot sizes at the mirrors to avoid damage to the coatings on the mirror faces, as was seen on the vacuum window coatings, and the laser light will be absorbed by the laser dump which will reside outside of the interaction region. The overall effectiveness of the design is limited by mirror coating technology and the space constraints in and around the HEBT interaction region. In the end, we expect that proving long pulse stripping will make the application of a laser stripping scheme a viable replacement of the graphite or diamond foil stripping technology pushing the scientific community through boundaries not presently achievable with today's foil technology.

7 - References

1. C.J.Liaw, Y.Y. Lee, and J. Tuozzolo, "Life Time of Carbon Stripping Foils for the Spallation Neutron Source, PAC 2001, Chicago, IL, 2001.
2. R.Shaw, M.A. Plum, LL.Wilson, C.S. Feigerle, M.J. Borden, T. Spickermann, Y. Irie, I. Sugai, and A. Tagaki, "Spallation Neutron Source (SNS) Diamond Stripper Foil Development", PAC 2007, Albuquerque, NM, 2007, p.620-622.
3. J. Beebe-Wang, Y. Y. Lee, D. Raparia, and J. Wei, "Injection Carbon Stripping Foil Issues in the SNS Accumulator Ring", PAC 2001, Chicago, IL, 2001
4. V. Danilov, A. Aleksandrov, S. Assadi, S. Henderson, N. Holtkamp, T. Shea, and A. Shishlo, "Three-step H⁻ charge exchange injection with a narrow-band laser", Phys. Rev. ST Accel. Beams **6**, 053501 (2003).
5. J. Beebe-Wang, Y. Y. Lee, D. Raparia, J. Wei, J., C. R. Prior, and S. Machida, "Beam Properties in the SNS Accumulator Ring Due to Transverse Phase Space Painting", Proceedings of the EPAC 2000, Vienna, Austria, 26-30 June 2000, p.1465-1467.
6. A. Zelensky, S.A. Kokohanovskiy, V.M. Lobashev, N.M. Sobolevskiy, and E.A. Volferts, Nucl. Instrum. Methods., Sect. A, **227**, **429-433** (1984).
7. I. Yamane, "H⁻ charge-exchange injection without hazardous stripping foils", Phys. Rev. ST Accel. Beams **1**, 053501 (1998).
8. M. A. Furman, "Lorentz Stripping of H⁻ Ions", LBNL-42722/CBP Note-287 (1999).
9. Leonard R. Scherk, "An Improved Value for the Electron Affinity of the Negative Hydrogen Ion", Can. J. Phys. **57**, 558 (1979).
10. A. J. Jason, D. W. Hudgings, and O. B. van Dyck, "H⁻ Field Detachment", IEEE Trans. Nucl. Sci. **28**, 2704 (1981).
11. V. Danilov, A. Aleksandrov, S. Assadi, J. Barhen, W. Blokland, Y. Braiman, D. Brown, C. Deibele, W. Grice, S. Henderson, J. Holmes, Y. Liu, A. Shishlo, and A. Webster, "Proof-of-principle demonstration of high efficiency laser-assisted H⁻ beam conversion to protons", Phys. Rev. ST – Accel. Beams **10**, 053501 (2007).
12. V. Danilov, A. Aleksandrov, S. Assadi, J. Barhen, Y. Braiman, D. Brown, W. Grice, S. Henderson, J. Holmes, Y. Liu, and A. Shishlo, "First Results of SNS Laser Stripping Experiment", EPAC 2006, Edinburgh, UK, 2006.
13. M. A. Furman, "Lorentz Stripping of H⁻ Ions", LBNL-42722/CBP Note-287 (1999).
14. C.L. Pekeris, "Ground State of Two-Electon Atoms", Phys. Rev. **112**, 1649 (1958).
15. N. Drakos, Computer Based Learning Unit, University of Leeds (1993, 1994, 1995, 1996).
16. M.G. Littman, M.M. Kash, and D. Kleppner, "Field-Ionization Process in Excited Atoms", Phys. Rev. Lett. **41**, 103 - 107 (1978).
17. I. Dickmann – Fachbereich Physikal. Technik, Experiment 03 – Fabry Perot Resonators (2003)